Direct Spectroscopic Observation of the Structural Origin of Peroxide Generation from Co-Based Pyrolyzed Porphyrins for ORR Applications

Joseph M. Ziegelbauer,[†,⊥] Tim S. Olson,[‡] Svitlana Pylypenko,[‡] Faisal Alamgir,[§] Cherno Jaye,[||] Plamen Atanassov,[‡] and Sanjeev Mukerjee*,[†]

Northeastern University, Department of Chemistry and Chemical Biology, 360 Huntington Avenue, Boston, Massachusetts 02115, University of New Mexico, Department of Chemical and Nuclear Engineering, 209 Farris Engineering Center, Albuquerque, New Mexico 87131, Georgia Institute of Technology, Materials Science and Engineering, 771 Ferst Drive NW, Atlanta, Georgia 30332, and National Institute of Standards and Technology, Ceramics Division, 100 Bureau Drive, Gaithersburg, Maryland 20899

Received: January 8, 2008; Revised Manuscript Received: March 31, 2008

Pyrolyzed transition metal based porphyrins present an attractive alternative to state of the art Pt-based electrocatalysts for fuel cell applications based on their comparatively low cost. Unfortunately, the large array of precursors and synthetic strategies has led to considerable ambiguity regarding the specific structure/property relationships that give rise to their activity for oxygen reduction. Specifically, considerable debate exists in actual chemical structure of the pyrolyzed reaction centers, and their relationship to membrane-damaging peroxide yield. In this manuscript a comprehensive electrochemical and spectroscopic study of pyrolyzed CoTMPP produced via a self-templating process is presented. The resulting electrocatalysts are not carbon-supported, but are highly porous self-supported pyropolymers. Rotating ring disk electrode measurements showed that the materials pyrolyzed at 700 °C exhibited the highest performance, whereas pyrolysis at 800 °C resulted in a significant increase in the peroxide yield. X-ray photoelectron spectroscopy and Co L and K edge extended X-ray absorption fine structure (EXAFS) studies confirm that the majority of the $Co-N_4$ active site has broken down to $Co-N_2$ at 800 °C. Application of $\Delta\mu$ analysis (an X-ray absorption near-edge structure difference technique) to the in situ Co K edge EXAFS data allowed for direct spectroscopic observation of the geometry of O_{ads} on the pyropolymer active sites. The specific geometrical adsorption of molecular oxygen with respect to the plane of the $Co-N_x$ moieties highly influences the oxygen reduction reaction pathway. The application of the $\Delta\mu$ technique to other transition metal based macrocycle electrocatalyst systems is expected to provide similarly detailed information.

1. Introduction

The current state of the art cathode electrocatalyst materials for polymer electrolyte fuel cells (PEMFCs) are largely based on platinum (Pt and Pt alloys). Pt exhibits superb activity for oxygen reduction reaction (ORR) but suffers from several drawbacks. For example, Pt is also extremely reactive toward a variety of contaminants such as halide anions,[1] methanol (crossover),[2] carbon monoxide/carbon dioxide (via reverse water gas shift reaction), and ubiquitous organics.[3,4] The presence of these contaminants generally results in the extreme depolarization of a Pt-based cathode on the order of ~150−300 mV thus greatly reducing the target power output. To some extent, these issues have been mitigated by the introduction of Pt−M (M = transition metal) alloys.[5,6] However, Pt remains a rare and expensive noble metal, and this will forever hamper its adoption on a large scale.

The search for alternative materials for PEMFC cathodes is essentially centered around two main points: (1) reducing the overall cost of the electrode by eliminating expensive metals and (2) maintaining activity in the presence of Pt-depolarizing chemicals (e.g., methanol). Many efforts have been directed toward the development of metal carbides,[7–9] transition metal based chalcogenides,[10,11] and biological mimics.[12] The biological mimics possess a developmental history of these alternative materials and have been examined thoroughly for ORR applications in both acidic and alkaline media.[13]

Many biological processes are efficiently regulated by porphyrin-type active sites in proteins. Unfortunately, removing these active sites from the safety of the surrounding protein/enzyme, and directly plunging them into environmental conditions in which they were never meant to operate (various pH and temperature conditions), leads to several serious disadvantages. Primarily, full scale organometallic mimics (transition metal TPP, TMPP, OEP, etc.) lack acceptable long-term stability.[13] Further, while safely ensconced within a protective protein shell under biological environments (specific pH and ~37 °C operating temperatures) these active sites exhibit essentially 100% efficiency toward $4e^-$ ORR,[14] but they tend to skew toward the $2e^-$ (hydrogen peroxide) pathway under PEMFC conditions.[15]

These issues have been mitigated by pyrolyzing carbon-supported porphyrin precursors.[16–20] This process not only increases the stability of these materials in PEMFC conditions but also substantially skews the ORR process toward the $4e^-$ pathway.[21] Unfortunately, the incredible variety of pyrolysis conditions, precursors, and synthetic procedures has resulted

* To whom correspondence should be addressed. E-mail: s.mukerjee@neu.edu. Phone: (617) 373-2382. Fax: (617) 373-8949.
[†] Northeastern University.
[‡] University of New Mexico.
[§] Georgia Institute of Technology.
[||] National Institute of Standards and Technology.
[⊥] Current address: General Motors R&D Center, MC: 480-102-000, 30500 Mound Road, Warren, MI 48090.

10.1021/jp8001564 CCC: $40.75
Published on Web 05/21/2008

in ambiguity of the respective active site. In particular, there is much debate regarding the specific chemical structure of the pyrolyzed porphyrin active site responsible for the $4e^-$ ORR pathway.[22–25] Efforts to elucidate the structure are further complicated by the heterogeneity of the metal−nitrogen structures created by the pyrolysis process. Further, it has been reported that the support (i.e., specific variety of carbon black) not only plays an important part in the final structure of the pyrolyzed porphyrin center,[26] but also may contribute to the overall peroxide yield in its own right.

X-ray absorption spectroscopy (XAS) provides a powerful set of tools toward elucidating the specific structure/property relationships that give rise to these effects. XAS, a core level spectroscopy, is element specific. Further, as a short-range order technique (extended X-ray absorption fine structure or EXAFS), it is ideally suited to elucidating the inherent amorphicity of these materials. Utilization of the X-ray absorption near-edge spectroscopy (XANES) region allows for direct correlation of electronic states with local site symmetry.[5] It is the availability of high intensity synchrotron sources of X-ray radiation which allows XAS to be performed on electrocatalysts under in situ and in operando conditions.[5] Despite these advances, XAS has been of traditionally limited utility for these systems, for it is inherently a bulk-averaging technique. Recent advances in the analysis of in situ XANES data, however, have offered a new opportunity for in operando spectroscopic insight into electrocatalysis.[27,28]

The $\Delta\mu$ technique is essentially a "ΔXANES" process which utilizes unique normalization parameters to remove the bulk absorber signal and thereby allows for the direct spectroscopic observation of adsorbates on an electrocatalyst surface.[27] The requirements for in situ data collection are such that full EXAFS and XANES data are collected simultaneously, and the $\Delta\mu$ process serves as an ancillary analysis to standard XAS structure/property determinations. Initial reports were based on Pt/C electrocatalysts[27,28] and were able to offer direct spectroscopic proof of the geometric adsorption of H_{ads} and $O(H)_{ads}$ on the electrocatalyst surface. Further investigations extended the technique to Pt−M alloy (M = Cr, Fe, Co, or Ni) cathode electrocatalysts,[29] where water activation investigations provided unprecedented spectroscopic insight into the bifunctional effect.[5] These studies were further extended to half-cell[30] and operating PEMFC[31] studies of anode electrocatalysts (i.e., Pt−Ru), which correlated methanol decomposition and CO_{ads}.[30,32] The $\Delta\mu$ technique was further applied to a novel mixed phase chalcogenide electrocatalyst (De Nora's Rh_xS_y/C)[33,34] and proved to be the key to not only elucidating the pertinent active phase (Rh_3S_4) but also to providing for the first direct spectroscopic evidence of oxo-species adsorption in respect to electrochemical potential.[33,34]

In this report we discuss the results of applying the $\Delta\mu$ technique to in situ Co K Edge XAS data on self-supported pyrolyzed CoTMPP electrocatalysts developed by the University of New Mexico. These materials represent a significant extension of the $\Delta\mu$ technique, for these systems are far less defined than the periodic electrocatalytic surfaces of Pt[27–29] and Rh_xS_y-based[33,34] electrocatalyst systems. Three sets of electrocatalysts (pyrolyzed at 600, 700, and 800 °C, respectively) were electrochemically characterized via rotating ring disk electrode (RRDE) measurements and PEMFC tests to measure the overall kinetics and performance of these catalysts for ORR in acid electrolyte. Techniques such as X-ray photoelectron spectroscopy (XPS), high-resolution transmission electron microscopy (HRTEM), and Co $L_{2/3}$ edge near-edge X-ray absorption fine structure (NEXAFS) were employed to elucidate the bulk structural and electronic characteristics of the electrocatalysts. Following this rigorous examination of the system, the $\Delta\mu$ analysis was utilized to illustrate a direct structure/property relationship between the extent of Co−N coordination and the peroxide yield. To our knowledge this is the first time a metal organic reaction center has been investigated wherein the actual adsorption modes of oxygen are determined as a function of variation of metal−nitrogen coordination under actual cell operating conditions. This therefore forms the basis of further investigations on analogous systems for the eventual design of metal organic structures for efficient oxygen reduction reaction.

2. Experimental Section

2.1. Synthesis. 5,10,15,20-Tetrakis(4-methoxy-phenyl)21H, 23H porphyrine cobalt(II) (CoTMPP, Aldrich) was dissolved in tetrahydrofuran and mixed in a 1:1 mass ratio with Cab-o-Sil amorphous silica (Cabot Corporation). The solvent was allowed to evaporate, inducing precipitation of the catalyst precursor on the silica template. The silica-supported porphyrins were then pyrolyzed under a 100% nitrogen flow at 600, 700, or 800 °C. Following the pyrolysis, the silica template was removed via a potassium hydroxide wash, and the catalyst was air dried.

2.2. Structural Analysis. ***2.2.1. TEM.*** TEM images were acquired with a JEOL 2010 high-resolution transition electron microscope. The TEM was interfaced with a GATAN TV, Slow-Scan Cameras/Digital Micrograph System, and an Oxford LINK ISIS Energy Dispersive X-ray Spectroscopy System (Ultrathin Window). The sample was supported on a copper/carbon grid.

2.2.2. XPS. Surface composition of the as-synthesized pyrolyzed CoTMPP electrocatalysts was probed via XPS by utilizing a Kratos Axis Ultra spectrometer with a hemispherical energy analyzer and monochromatic Al Kα source. The high-resolution spectra of the Co2p, N1s, C1s, and O1s edges were acquired with a pass energy of 20 eV. All spectra were smoothed prior to background (linear for N1s, C1s, and O1s and Shirley for Co2p) subtraction. Calibration was performed by setting the aliphatic carbon peak to 285 eV. Spectra were decomposed using 70/30% Gaussian/Lorentzian peaks with widths constrained to 1.4, 1.0, 1.0, and 1.3 eV for Co2p, N1s, C1s, and O1s, respectively. Only the higher intensity $2p^{3/2}$ components of the Co2p were curve fitted. Data analysis and quantification were performed using CasaXPS software (2005 Casa Software Ltd.).

2.3. Electrochemistry. ***2.3.1. RRDE Measurements.*** All RRDE measurements utilized a Pine Instrument Co. rotator (model AFMSRX) and a RRDE comprised of a 5.6 mm diameter (0.246 cm^2 geometric) glassy carbon (gc) disk and Au ring. The experiments were potentiostatically controlled with an Autolab (PGSTAT30) potentiostat/galvanostat (Brinkmann Inc.). Prior to deposition of the ink, the gc was successively polished to a mirror finish with 1.0 and 0.05 μm alumina slurry (Buehler, Inc.). The collection efficiency of the Au ring was determined from the ferricyanide couple according to standard procedures.[35] All experiments were performed in 1 M perchloric acid (triply distilled, GFS Chemical Co.) with a Pt mesh serving as the counter electrode. The reference electrode was a sealed RHE generated from 1 M $HClO_4$ to eliminate junction potentials. All potentials are referred to the RHE (V vs H/H^+).

Catalyst inks were comprised of 1:1 (wt %) 2-propanol (HPLC grade, Alfa Aesar) and deionized water (Megapure, Millipore), the appropriate amount of dry catalyst, and a small amount of 5 wt % Nafion (Sigma Aldrich) as a binder. The total dry mass ratio of the catalyst to Nafion was 1:50, thereby allowing for the neglect

of additional diffusion terms.[35,36] The inks were applied to the gc via two successive 7-μL depositions followed by drying in dry air. Because the true mass of Co in the three catalysts was extremely low (3−8 wt % Co), all loadings are normalized to the total mass of the CoTMPP pyropolymer deposited on the gc (in all cases 55 μg total pyropolymer per 0.246 cm^2 geometric area).

The catalysts were activated by cycling between 1.0 and 0.02 V until a steady state voltammogram was achieved (typically ∼20 cycles). ORR curves (100, 400, 625, 900, 1225, and 1600 rpm) were collected at a slow scan rate of 10 mV s^{-1} in an effort to reduce the substantial double layer exhibited by all of the pyropolymers. Peroxide yields were determined by measuring the current observed at the Au ring when held at 1.3 V.

2.3.2. Fuel Cell Tests. The fuel cell testing was preformed on a Fuel Cell Technologies test station. The hand-painted 5 cm^2 MEA consisted of an 8 mg cm^{-2} PtRu anode, a 4 mg cm^{-2} CoTMPP pyrolyzed at 700 °C cathode, and a Nafion 1135 polymer electrolyte membrane (Du Pont) separator. Approximately 90% of cathode ink was applied to the microporous layer of the gas diffusion material (ELAT GDL LT 1400-W, BASF Fuel Cell Inc.). The balance of the cathode ink was applied directly to the Nafion membrane. The MEA was hot pressed at 1500 lbs and 125 °C for 5 min. All tests were performed in an H_2/air environment. The cell temperature was maintained at 80 °C with the humidification bottles measured at 85 °C. The H_2/air flow rates were 266 and 466 sccm, respectively, and at a constant 30 psi back pressure.

2.4. XAS Analysis. ***2.4.1. Ex Situ Co $L_{2/3}$ Edge NEXAFS.*** All tests were conducted at beamline U-7A of the National Synchrotron Light Source (NSLS, Brookhaven National Laboratories, Upton, NY) under near-ultrahigh vacuum conditions. As-synthesized catalyst powders were hand pressed onto sticky copper foil on the sample bar. The acid-washed samples consisted of electrodes (CoTMPP pyropolymer hand painted onto carbon cloth, Zoltek Companies, Inc.) that were soaked in 1 M $HClO_4$ for at least 4 h prior to rinsing with megapure deionized water. For comparative purposes a 30 wt % Co/VXC72 (E-TEK Inc., now BASF Fuel Cell) electrode was also examined. NEXAFS measurements at the Co L_2 and L_3 edges (793.2 and 778.1 eV, respectively) were collected at the National Synchrotron Light Source (NSLS) at the NIST soft X-ray beamline (U-7A), which is equipped with a Toroidal Mirror Spherical Grating Monochromator (TSGM). All the samples were mounted on an electrically grounded bar and examined using ultrasoft XAS over the range of 700−900 eV. The U-7A experimental chamber provides for measurements of surface sensitive partial electron yield (PEY) intensities utilizing a channeltron with a three grid high pass electron kinetic energy analyzer. All NEXAFS measurements were made with the photon beam approximately at the magic angle (∼35°) to the sample surface normal while maintaining the grid high pass bias at −150 V. A 1200 lines mm^{-1} monochromator grating and 30 μm entrance/exit slits were used, providing an energy resolution of 0.3 eV in the energy range 700 − 900 eV. All data acquisition was performed in conjunction with a CoFeNiCr mesh to aid in energy calibration. Designation of the edge energies and normalization of the spectra were performed with the IFEFFIT suite.[37] The spectra were deconvoluted by using the minimum number of Gaussian functions in conjunction with a single step (arctan) function in an iterative fitting procedure. Fitting of the Gaussians was accomplished with the WinXAS code.[38]

2.4.2. In Situ Co K Edge XAS. The in situ Co K edge XAS measurements were performed at NSLS beamline X-23A2 utilizing a previously described cell design.[33,39] The 5 cm^2 working electrodes consisted of 95:5 wt % pyropolymer:Nafion binder hand painted onto commercially available carbon cloth (Zoltek). While the total geometric loading of the Co in the working electrodes was chosen to give a transmission adsorption height of ∼0.2 (assuming 10 wt % Co in the catalyst powders) all data was collected in the fluorescence mode with a single PIPS detector in an effort to keep the electrode at a reasonable thickness. A Nafion 112 membrane (Du Pont) acted as the separator, and a thin 0.5 mm Au wire (99.995%, Alfa Aesar) was utilized as the counter electrode. As with the RRDE experiments, a sealed RHE, generated from identical 1 M $HClO_4$ electrolyte, was used as the reference electrode, and all potentials are reported relative to the RHE. Prior to cell assembly, the working electrodes were vacuum soaked in deaerated 1 M $HClO_4$ electrolyte for 2 h followed by a light rinse with megapure deionized water. The electrolyte was deaerated via bubbling with $Ar_{(g)}$ for at least 20 min prior to introduction into the cell to remove any interference (i.e., molecular oxygen) toward the water activation process.

The catalysts were activated by cycling 3−5 times between 0.02 and 1.0 V at 20 mV s^{-1} utilizing a model PGSTAT30 Autolab potentiostat/galvanostat. Following activation, full Co K edge EXAFS scans (−200 eV to 14k) were collected in 100 mV intervals from 0.30 − 1.00 V on successive anodic sweeps. For the 700 °C pyrolyzed electrocatalyst, an additional potential (1.2 V) was collected following the conclusion of the 0.30−1.00 V regime. All measurements were collected in conjunction with a thin Co foil to aid in energy alignment. All EXAFS normalization and fitting[40] were performed with the IFEFFIT suite (version 1.2.8).[37]

The process of the $\Delta\mu$ analysis has been described in detail in prior publications[27,28,33] and will only be briefly summarized here. Following a careful energy alignment and background removal of the scans, the absorption spectra were normalized from just past the white line to ∼120 eV past the edge. The $\Delta\mu$ signals were generated according to the relationship

$$\Delta\mu = \mu(\mathrm{V}) - \mu(0.30\mathrm{V}) \quad (1)$$

where the signal at 0.30 V was determined to be the "cleanest" (adsorbate free) potential via electrochemical and standard EXAFS analysis. Interpretation of the $\Delta\mu$ signals was achieved by constructing models via CAChe (v. 6.1.12, Fujitsu Computer Systems Incorporated) of $Co-N_x$ ($x = 2$, 3, or 4) with molecular oxygen adsorbed in different positions. These models were based on both literature parameters[24,41−43] in addition to the results of the experimental EXAFS analysis. Theoretical XANES spectra of these models were then generated with the FEFF8 code.[44] These signals were then subjected to the same difference process utilized for the experimental data according to the following relationship

$$\Delta\mu = \mu(\mathrm{Co}-\mathrm{N}_x-\mathrm{O}_{ads}) - \mu(\mathrm{Co}-\mathrm{N}_x) \quad (2)$$

3. Results and Discussion

3.1. Characterization. ***3.1.1. TEM Studies.*** A representative TEM micrograph of the as-synthesized nonsupported templated pyrolyzed (700 °C) electrocatalyst is presented in Figure 1. Graphitelike planes dominate the micrograph and illustrate the porosity of the final material. The inset in the upper left corner illustrates the chemical composition of the pyropolymer after minimal decomposition and provides a reasonable interpretation of the origin of the planes in the micrograph. In reality, the resulting pyropolymer is not flattened akin to the upper left inset but is "balled up". A three-dimensional representation of the porous carbon structure of the pyropolymer is shown in the inset

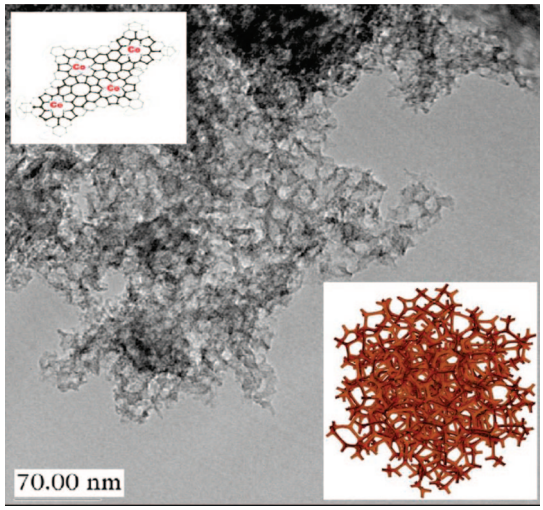

Figure 1. TEM micrograph of the prepared CoTMPP pyropolymer following 700 °C thermal treatment. Top left inset: flattened schematic of $Co(N_4C_{24})_4$. Bottom right inset: space-filling model of the porous pyropolymer.

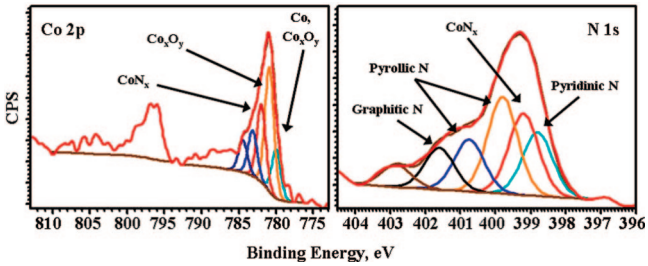

Figure 2. Representative Co2p (left) and N1s (right) CoTMPP 700 °C XPS data and fitting.

at the lower right in the micrograph. These TEM studies illustrate the unique morphology of the pyrolyzed CoTMPP-based electrocatalyst produced via this unique self-templating process.

3.1.2. XPS Analysis. The structure of pyrolyzed porphyrins has been studied for years, and it is well-known/documented that their composition undergoes complex changes during pyrolytic synthesis.[45] A thorough XPS characterization of the composition of the CoTMPP precursor and pyrolyzed CoTMPP electrocatalysts (at various temperatures) is published elsewhere.[45] Combination of XPS and multivariate analysis utilized in the prior report allowed for enhanced identification of moieties and transformations arising from pyrolysis. It was concluded that partial decomposition of the porphyrin macrocycle ring during the pyrolysis leads to formation of carbon−nitrogen polymeric-like network. It is believed that the as-synthesized catalysts (pyrolyzed at 600 °C and above) possess Co metal distributed between the carbonaceous pyropolymer network and the nanoparticle decorated phase.

High-resolution Co2p and N1s spectra of CoTMPP pyrolyzed at 700 °C, shown in Figure 2, demonstrate the complexity of the composition of the pyrolyzed material. Analysis of Co2p spectra reveals that part of the cobalt is still associated with nitrogen (peak at 782 eV), while another part of the cobalt released from Co−N_x centers form particles of metallic cobalt covered by cobalt oxides (peaks at 780 and 780.9 eV in Co2p). Curve fitting of N1s confirms that part of the cobalt is still coordinated with nitrogen (peak at 399.2 eV). The rest of nitrogen is converted into pyridinic, pyrollic, and graphitic nitrogen species.

TABLE 1: Electrocatalyst Structural Parameters Determined via ex Situ XPS and in Situ EXAFS

catalyst	ΔE, eV (XANES)	$N_{N/Co}$ (XPS)	$N_{N/Co}$ (EXAFS)[b,c]	$N_{O/Co}$ (EXAFS)[b,c]	R_{Co-N}, Å (EXAFS)[b,c]
600 °C	5.00	2.7	3.1	1.2	1.904
700 °C	5.34	2.6	2.8	1.2	1.906
800 °C	5.53	1.5	1.4	1.1	1.890
Co(II)OEP[a]	4.89		3.6	0.8	1.965

[a] Unpyrolyzed, +99.5% pure, ex situ XAS scans. [b] In situ XAS conditions: 0.60 V, Ar-saturated 1 M $HClO_4$. S_0^2 fixed at 0.78 (via FEFF); σ^2 fixed at 0.003 Å^2; fitting of the k^1-weighted Fourier transform, k range 0.9−10 Å^{-1}, R range 1.0−3.4 Å. E_0 and χ^2 ranges were −1.1 to +5.5 eV and + 849 to +155, respectively. [c] XAS fitting error: $N \pm 20\%$; $R \pm 0.02$ Å.

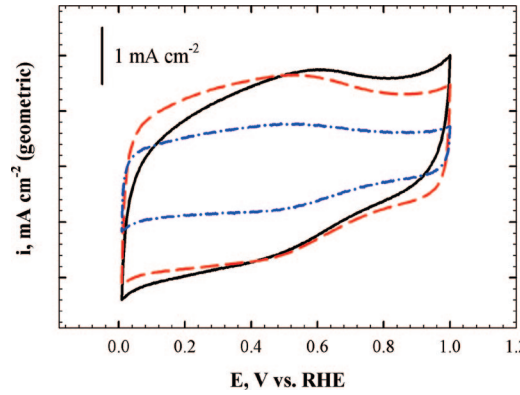

Figure 3. Comparison cyclic voltammograms of the 600 (solid line), 700 (dashed line), and 800 °C (dash−dotted line) pyrolyzed CoTMPP electrocatalysts in room-temperature Ar-saturated 1 M $HClO_4$. Scan rates: 50 mV s^{-1}. Total pyropolymer loadings: 55 μg per 0.246 cm^2.

The quantities of cobalt and nitrogen atoms that retained a porphyrin-type Co−N_x structure were determined from quantification of Co2p and N1s spectra, respectively. N/Co coordination numbers of 2.7, 2.6, and 1.5 were obtained for the materials pyrolyzed at 600, 700, and 800 °C, respectively (Table 1). The number of nitrogen atoms per cobalt atom decreases with the increase in pyrolysis temperature. This observation is consistent with the overall decomposition of the material. It can be speculated that at 600 and 700 °C the predominant coordinations are Co−N_4 and Co−N_2. At higher temperatures Co is predominantly coordinated as Co−N_2 and Co−N.

At all temperatures, the XPS results present unambiguous evidence of nanoscale hexagonal cubic packing (hcp) metallic Co and Co oxides. As XPS is a surface sensitive technique, it is obvious that these domains reside on the surface of the pyropolymer. This analysis therefore provides the justification for the overall surface morphology of the as-synthesized electrocatalysts. It is estimated that approximately half of the silica-supported CoTMPP results in surface deposits of nanoscale Co metal and oxides. The remaining porphyrin material is present in the form of Co−N_x, where $x = 1-4$. All of these materials are supported on a balled-up graphitic matrix of carbon. While XPS is surface sensitive, and this overall analysis is essentially a "bulk average" of the surface characteristics, these results have proven to be of significance in defining the as-synthesized morphology of the Cobased pyropolymers produced by this unique synthetic methodology.

3.2. Electrochemistry. ***3.2.1. RRDE.*** Cyclic voltammograms of the three catalysts in Ar-saturated 1 M $HClO_4$ are presented in Figure 3. The scans for all three catalysts are dominated by a large double-layer capacitance arising from the underlying pyropolymer. Further, the slight redox feature

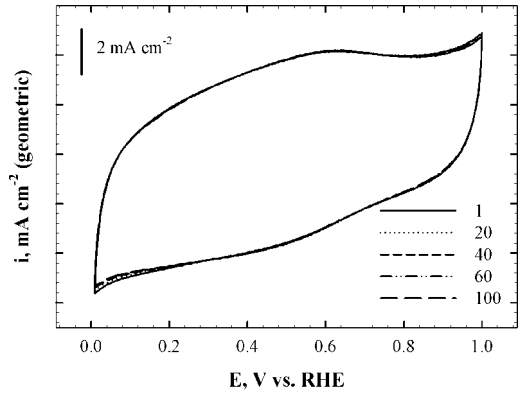

Figure 4. 100 scans of CoTMPP (700 °C) in room-temperature Ar-saturated 1 M $HClO_4$. Scan rate: 50 mV s^{-1}. Total pyropolymer loading: 55 μg per 0.246 cm^2.

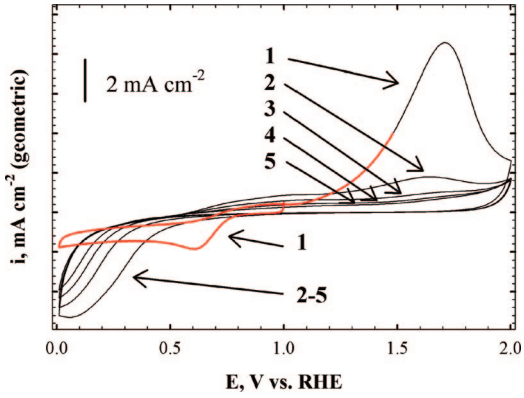

Figure 5. CoTMPP (700 °C) in room-temperature O_2-saturated 1 M $HClO_4$. Scan rate: 50 mV s^{-1}. Total pyropolymer loading: 55 μg per 0.246 cm^2.

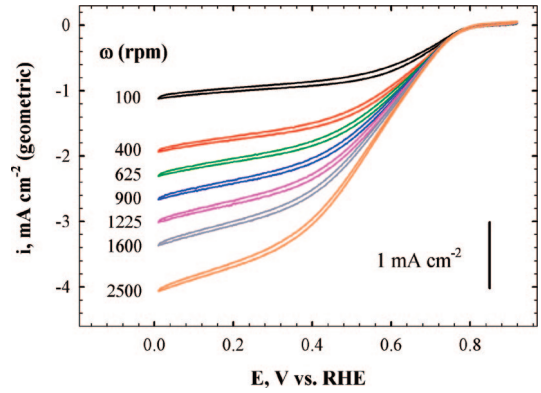

Figure 6. Representative complete ORR curves for CoTMPP (700 °C) in room-temperature O_2-saturated 1 M $HClO_4$. Scan rate: 10 mV s^{-1}. Total pyropolymer loading: 55 μg per 0.246 cm^2.

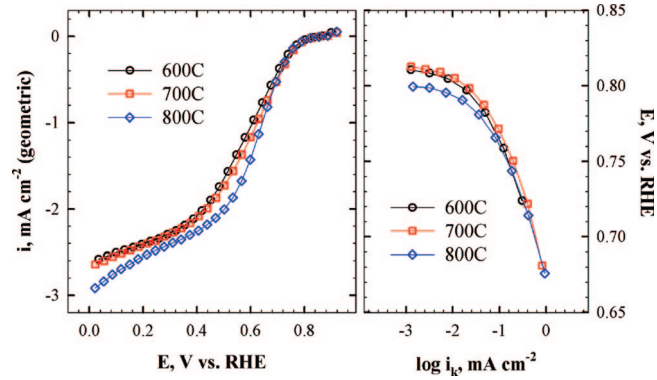

Figure 7. RRDE comparisons of the three electrocatalysts in room-temperature O_2-saturated 1 M $HClO_4$. Scan Rates: 10 mV s^{-1}. Left: normalized ORR curves at 900 rpm. Right: Mass transfer corrected Tafel Plots at 900 rpm.

centered at ~0.50 V can be easily assigned to the carbon-based pyropolymer backbone akin to the more common hydroquinone features sometimes observed with carbon black-supported electrocatalysts. None of the materials show clear evidence of a Co redox couple. Pyrolyzing the Co(II)TMPP precursor at 800 °C results in comparatively large reduction in the magnitude of the double layer suggesting that the surface area and/or porosity of the electrocatalyst has been greatly reduced. The electrocatalysts can be considered to be stable on the basis of long-term cyclic voltammetry (Figure 4).

In an effort to discern the chemical nature of the reaction center, the electrocatalysts were subjected to cyclic voltammetry in O_2-saturated 1 M $HClO_4$ over a wide electrochemical window (Figure 5). Polarizing the electrocatalysts to 2.0 V resulted in large, irreversible anodic peaks at ~1.8 V. Upon successive returning cathodic sweeps, the reduction feature shifts to increasingly negative potentials. The large anodic peak at 1.8 V can be assigned to the irreversible oxidation of Co to the 3+ oxidation state. Loss of the Co center effectively ruins the performance of the electrocatalyst thus indicating that Co is the ORR-active center in these materials.

The ORR curves in 1 M $HClO_4$ for the 700 °C catalyst are presented in Figure 6 and are characteristic of all three electrocatalysts. A well-defined limiting current is observable at all rotation rates, and the Levich relation is maintained. Further, the reduction curves are singular in nature thus indicating a single reaction site and reduction process. The cathodic ORR sweeps at 900 rpm for all three electrocatalysts are compared in Figure 7. Regardless of the pyrolysis temperature, all the electrocatalysts possessed an ORR onset potential of ~0.80 V (Table 2). By performing a first-derivative analysis of the ORR curves, the limiting current was designated at 0.30 V (where the slope became constant). Utilizing the limiting current densities allowed for the determination of the mass transfer-corrected Tafel Plots (Figure 7, right). From the derived kinetic parameters (Table 2) the performance of the electrocatalysts can be ranked as 700 > 600 > 800 °C.

Akin to other reports,[46,47] the electrocatalysts in this study were found to exhibit low Tafel slopes similar to the 60 mV dec^{-1} region observed with Pt/C electrocatalysts. For Pt-based electrocatalysts, these values are interpreted as the first electron transfer being the rate-determining step (under Temkin absorption isotherm conditions).[4,48] This similarity suggests that the porphyrin materials accomplish ORR in a manner similar to Pt/C. These observations are bolstered by the derived Levich−Koutecky and reaction order plots (Figures S1 and S2 of Supporting Information, respectively). In the Levich−Koutecky plots, none of the electrocatalysts pass through the origin indicating that total diffusion control has not been obtained. This is most likely a result of the highly porous nature of the materials. Further, the 800 °C electrocatalyst shows nonparallel lines indicating that the number of electrons transferred is changing over the potential window. Examination of the derived reaction orders (Figure S2) provides a possible explanation for the deviation of the 800 °C pyropolymer. In general, the 600 and 700 °C catalysts reveal reaction orders of ~1.0, while the 800 °C material is noticeably higher at ~1.5−2.0. Further, it is notable that the peroxide yield (Table 2) of the 800 °C material is considerably higher than the other pyropolymers. While a peroxide yield of >3% is high in comparison to state of the art

TABLE 2: ORR Kinetics

pyrolysis temperature	OCP (V vs RHE)	E_{onset} (V vs RHE)	b (mV dec^{-1})	i_0 (mA cm^{-2})[a]	$\chi_{H_2O_2}$(0.60 V)
600 °C	0.845	0.810	23/83	2.30×10^{-7}	2.9
700 °C	0.884	0.806	30/81	6.38×10^{-6}	3.3
800 °C	0.868	0.796	25/72	5.49×10^{-8}	34.9

[a] Surface areas are geometric.

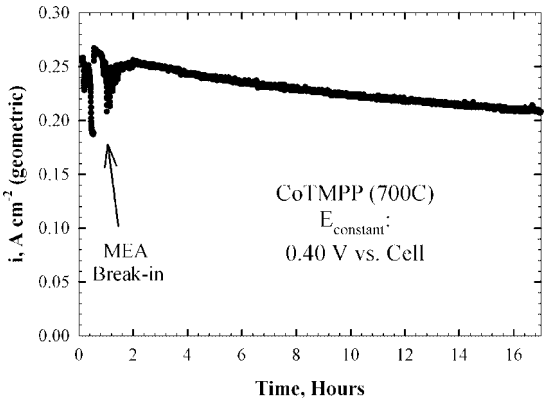

Figure 8. CoTMPP (700 °C) long-term H_2/air fuel cell evaluation at $E_{constant}$ = 0.40 V vs cell. See text for test parameters.

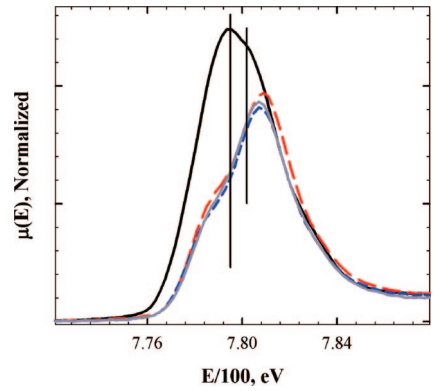

Figure 9. Normalized Co L_3 edge NEXAFS scans comparing the 30 wt % Co/C nanoparticles and the three pyrolyzed porphyrins electrocatalysts (as-synthesized/unwashed): Co/C (black solid line), 600 °C (long dash), 700 °C (short dash), and 800 °C (gray solid). The two vertical solid drop lines denote the positions of the two observed peaks in the Co/C spectrum.

Pt-based systems, it is notable that these numbers show that pyrolysis of porphyrin molecules greatly reduce these effects.[12] Overall, these observations suggest that the electrocatalyst resulting from the 800 °C pyrolysis possesses fundamentally different structural characteristics from its 600 and 700 °C brethren, and as a result the kinetic ORR pathway is skewed toward the 2e$^-$ route.

3.2.2. Fuel Cell Characterization. The extreme porosity of the pyropolymer electrocatalysts required a series of strategies to optimize the MEA for performance and stability. The cathode ink composition was varied in terms of catalyst, Nafion, and carbon black loading. Over 20 iterations were examined to find the optimal composition.[49] The details of this process are outside of the scope of this report, and will be published elsewhere. Figure 8 presents the results obtained with the highest-performing (700 °C pyrolysis) cathode composition.

When working with Pt-based materials, cost is always a concern, and therefore increasing the Pt utilization is a key issue. However, in cases where the cost of the electrocatalyst material does not contribute in any significant portion to the overall system cost, then the engineering goal is to increase active site density to increase the power output. On the basis of the results in Figure 8, the accessible site density would have to be increased on the order of 3−5 times to be comparable with Pt-based catalysts. Still the results expressed in Figure 8 are encouraging. It is clear that site density is limiting the performance, and strategies can be developed to address this issue. Further, this test has also addressed one of the major concerns regarding non-Pt catalyst for PEM applications; long-term stability. Here it is shown that the catalyst layer is at least stable for ∼15 h. Even if non-Pt materials do not meet the long-term stability requirements for automotive applications (∼5000 h of use) there are other foreseeable applications. For example, pyrolyzed macrocycles, such as CoTMPP, have been reported to exhibit appreciable methanol tolerance.[21,50] This property could allow a direct methanol fuel cell to operate at high methanol concentrations (≥10 M) that a Pt-based cathode could not support. Because the material costs of the pyropolymers are so low, it would be economically feasible to incorporate such a material in a system that utilizes a disposable cathode.

3.3. XAS Studies. ***3.3.1. Co $L_{2/3}$ Edge NEXAFS.*** The $L_{2/3}$-edges of 3d metals result from a dipole-allowed transitions from the 2p shell electrons to unfilled 3d states where the transition cross sections are proportional to the density of unoccupied 3d states under the constraints of a unique symmetry condition.[51] All of the spectra were deconvoluted using the minimum number of Gaussian functions together with a single step (arctan) function in an iterative fitting procedure with the aim of providing a unique fit. The Gaussians were constrained to have a full width at half maximum equal to one another under the assumption that each orbital (represented by an individual Gaussian) is sensitive to the same local disorder and are subject to the same core-hole lifetime broadening.[51]

The L_3 edge peaks of as-prepared and acid-washed porphyrin complexes of Co prepared by pyrolysis at different temperatures have been compared. The Co L_3 spectra from the Co pyropolymers were further contrasted to those of 30 wt % Co/C. The spectra of the different as-prepared porphyrin samples with the Co nanoparticles are shown, after background subtraction and normalization, in Figure 9. The two main peaks observed in the Co nanoparticles (marked by lines) fall between the main peaks of the as-synthesized pyropolymer electrocatalysts, indicating a markedly different local symmetry between the two. The two lines from nanoparticulate Co/C are contributions from both from Co^0 atomic states (from the particle cores) and Co^{2+} states from surface cobalt oxide,[51] where the higher position of the Co^{2+} peak results from a stronger Coulombic attraction overcome by photoexcited core−electrons from Co^{2+} species relative to that of the neutral Co species.

Three Gaussian functions were required to fit the L_3 peak shape of the porphyrin molecules. We can tentatively assign the lowest energy Gaussian, labeled G1 in Figure 10, with the d_{xy} orbital which has a single electron (d_{z^2}, d_{xz}, and d_{yz} being below the Fermi level with 2 electrons each for a d^7 cation). The second Gaussian (G2 in Figure 10) is then the $d_{x^2-y^2}$, which is fully unoccupied and therefore has approximately twice the area of G1. The third Gaussian, G3, is a minority feature that

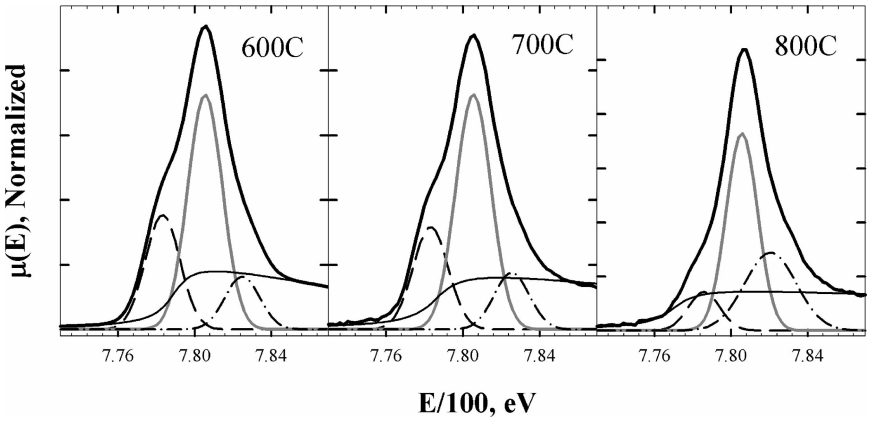

Figure 10. Co L_3 edge NEXAFS spectra of the washed porphyrins pyropolymers pyrolyzed at (left to right) 600, 700, and 800 °C. The Gaussians under the experimental curves are referred to in the text as G1 (dash), G2 (gray), and G3 (dash−dot). The thin solid black line in each spectrum represents the single step (arctan) function.

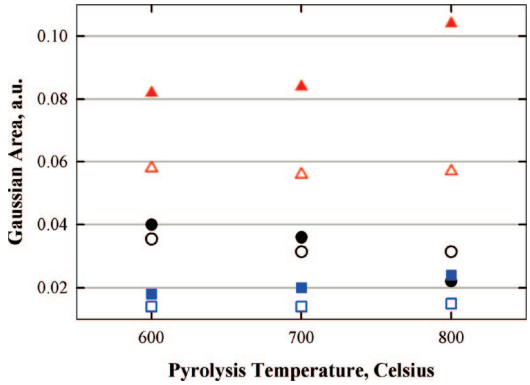

Figure 11. Areas of the three Gaussian peaks per pyrolyzed Co L_3 edge NEXAFS spectra plotted against pyrolysis temperature. As-synthesized spectra are represented by filled in symbols, whereas the acid-washed materials are denoted by unfilled symbols: G1 (circles), G2 (triangles), G3 (squares).

cannot acquire an orbital designation under this scheme, and it is speculated that it is a species from a non-square−planar local symmetry.[52] Figure 11 displays a comparison of the areas under G1, G2, and G3 in the as-prepared and acid-washed porphyrin molecules. The acid-washing step increases the areas under the Gaussians indicating that the acid-washing step has removed a significant amount of Co that is not in porphyrin molecules. The 800 °C process changes the ratio of G1 to G2, suggesting that the square planar configuration has been eliminated.

3.3.2. In Situ K Edge XAS. *3.3.2.1. XANES.* Representative in situ Co K edge XANES spectra of the electrocatalysts and standards at 0.40 V are presented in Figure 12. It is immediately apparent that the pre-edge features of the porphyrins differ significantly from that of the Co foil. For example, the Co(II)OEP material exhibits a 1s → 4p electron transition consistent with planar (D_{4h}/S_4 symmetry) molecules exhibiting a peak splitting of ∼5.5 eV.[53,54] To a certain extent, these transitions are still observable in the pyropolymers, although they are considerably muted (Figure 13 and Table 1) and decrease with higher pyrolysis temperatures. This suggests that the planar Co−N_4 structure is maintained to a certain extent but is being broken down by higher temperature heat treatments. In addition, it is worth noting that comparison of the absorption edge and the white line features to the Co foil standard reveals that the pyropolymers possess no metallic Co character. This is in contrast to the XPS results discussed in section 3.1.2. However, the XPS analysis was performed on as-synthesized powders, whereas the K edge XANES data was gathered under fully wetted *in operando* conditions. If nanoparticles of metallic Co (or CoO_x) were initially present on the surface of the pyropolymers, these particles seem to have been unable to survive the low pH environment of the electrochemical cell and have most likely dissolved into the electrolyte. These observations fully support the results of the Co $L_{2/3}$ analysis discussed in section 3.3.1.

The effect of the electrochemical potential on the XANES (for brevity only the CoTMPP 700 °C sample is presented) is shown on the right side of Figure 12. As expected, the absorption edge energy shifts to higher values with an increase in potential indicating an oxidation of the Co. The inset shows the change in the white line intensity with respect to potential. The white line intensity arises from the same 1s → 4p transition observed in the pre-edge region and provides insight into the change of the partial density of the final states above the Fermi level.[51] It is particularly notable that a sudden increase in the magnitude occurs at 0.80 V (the observed onset potential for ORR based on the previously discussed RRDE results). By the time that 1.0 V has been applied, the magnitude of the white line stabilizes up to 1.2 V. This suggests that a full complement of O_{ads} is present at 1.0 V. These conclusions are bolstered by the noticeable change in the small pre-edge feature at ∼7715 eV attributed to the A_{1g} transition. This feature is wholly dependent on the planar conformation of the molecule and is nearly wiped out by O_{ads} in what can be assumed to impart upon the catalyst center a quasi-octahedral symmetry.

3.3.2.2. EXAFS. Representative Fourier transform spectra (k^1 weighted, 0.40 V) for the examined electrocatalysts are presented in Figure 14. Akin to both the $\chi(k)$ (Figure S3 of Supporting Information) and raw absorption spectra, the pyrolyzed materials do not exhibit any appreciable features past 4 Å. In the FT spectra, all three materials display a large feature at ∼2 Å, and the peak maximum for the pyropolymers is located at slightly shorter atomic distance than the main peak for the Co(II)OEP standard. This main peak also provides evidence of a shoulder feature at 2+ Å with the Co(II)OEP showing appreciable definition.

The peak intensities are a combination of the Debye−Waller factor and coordination number. By ulitilization of published crystallographic parameters,[42,43] first and second coordination shells for the in situ data were performed (Figure 15 and Table 1). Co(II)OEP provides a perfect case scenario, for it has therefore lent itself to exhaustive structural characterization via its propensity for crystallization (an subsequent XRD analysis).[43] This material was, however, included in the study to provide a

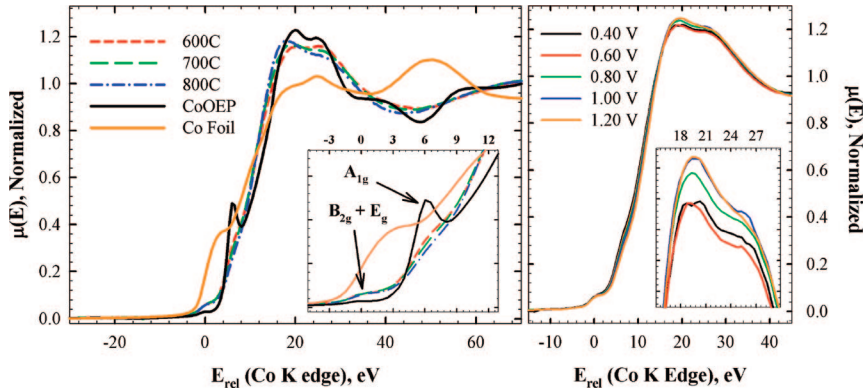

Figure 12. In situ Co K Edge (7709 eV) XANES spectra of the pyropolymer electrocatalysts in 1.0 M $HClO_4$. Left: 0.40 V vs RHE with the Co reference foil and unpyrolyzed (ex situ) Co(II)OEP overlaid. Right: CoTMPP (700 °C) XANES spectra in respect to the anodic potential.

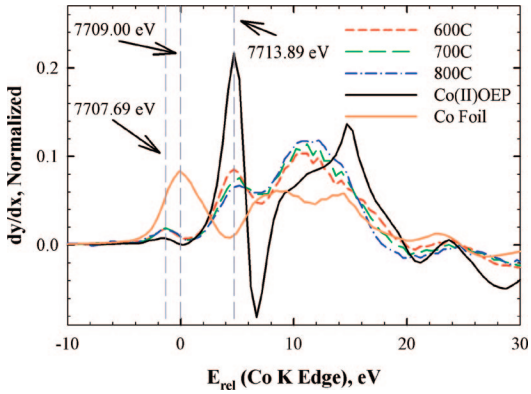

Figure 13. First-derivative analysis of the Co K absorption edge spectra presented in Figure 12 (left).

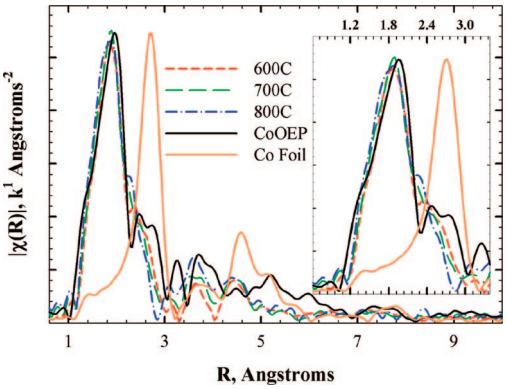

Figure 14. The k^1-weighted Fourier transforms of the three pyropolymer electrocatalysts at 0.40 V (anodic) with the ex situ Co(II)OEP powder and Co foil shown for reference.

well-established background for comparative purposes in regards to the phase mixture/speciation in pyrolyzed CoTMPP materials, and therefore only the relevant first two shell fits of the unpyrolyzed porphyrin polymer were performed. As expected, the primary low R peak arises from the 4 N molecules surrounding the absorbing Co center. The shoulder arises from second shell interactions of the carbon molecules (inset, Figure 15). As expected,[43] fitting of this ex situ data set showed that adsorbed oxygen was present.

Fitting the pyrolyzed porphyrin electrocatalysts proved to be far more difficult due to the mixed phase character resulting from the pyrolysis. Because of this ambiguity, only a first shell fit was deemed to be reasonable. It was verified that the primary initial peak arose from a mixture of N and O molecules coordinated in the first shell, for models of hcp Co metal and

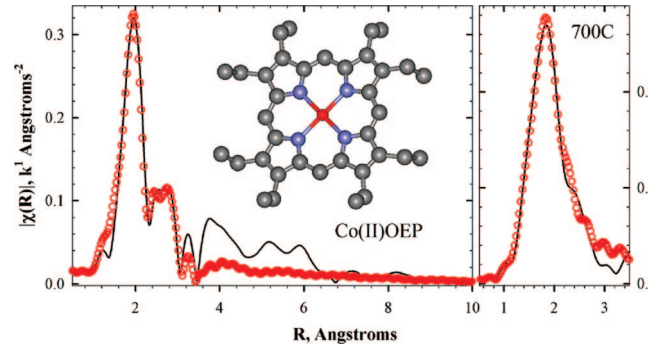

Figure 15. Representative k^1-weighted Fourier transform fits of ex situ Co(II)OEP (left) and in situ 700 °C CoTMPP at 0.40 V (right).

various CoO_x oxides did not fit the attained in situ spectra. These efforts resulted in values for Co−N coordination numbers (i.e., N_{Co-N}) that are not far removed from the XPS analysis of the ex situ (as-synthesized) electrocatalysts (Table 1). The bulk N_{Co-N} values are ~3 until pyrolysis was performed at 800 °C, upon which N_{Co-N} dropped to less than 2. It is notable that the N_{Co-N} values from the in situ XAS data analysis are slightly higher (Table 1) than those obtained for the ex situ XPS analysis, but the agreement is well within the error limits.

Refinement of the N_{Co-N} values showed that the average Co−N interatomic distance decreases for the pyrolyzed materials and is in agreement with literature reports.[24] In addition to Co−N interactions, the extent of N_{Co-O} as a function of potential was also explored. As expected, N_{Co-O} increases at higher potentials owing to oxidation of the active site. Most importantly it was verified that the N_{Co-O} value was essentially zero at 0.30 V. As all examined potentials were on the anodic sweep direction, these results indicate that the Co active center is essentially free of O_{ads} at 0.30 V following a full cathodic sweep to 0.02 V.

These results, in conjunction with the L edge data comparing "as-synthesized" and "acid-washed" samples, indicate several important aspects of the electrocatalysts. First, both the acid-washed and in situ materials are free from nanoparticles of metallic and/or Co oxides which are present as justified by the results from the ex situ XPS and Co L edge (on the "as-synthesized" electrocatalysts) experiments. Second, while it is not argued that the materials are homogeneous, the bulk EXAFS results suggest that a higher coordination of nitrogen to Co is present until a pyrolysis temperature of 800 °C is reached. Finally, these results show that the bulk, underlying electrocatalyst morphology does not change (in respect to potential) until unrealistically high operating/electrolytic potentials (i.e., above 1.00 V vs RHE) are reached.

However, EXAFS analysis of a mixed phase system is of limited utility, for XAS is, as a core level spectroscopy, inherently bulk averaging by nature. That is, while the bulk EXAFS-derived N_{Co-N} values for the 700 °C material are ~3, this does not lend any insight into whether the entirety of the material is planar Co−N_3 but instead should be considered as some sort of undeterminable mixture of Co−N, Co−N_2, Co−N_3, and Co−N_4. Indeed, despite reasonable calculated E_0 values for the fits, the "goodness of fit" parameter (reduced χ^2) was always above ~150 (and +1000 for the 800 °C material) thus indicating a less than perfect approximation of the chemical environment owing to indefinable levels of stoichiometric Co−N_x mixing. Additional data analysis techniques such as principal component analysis (PCA) and residual phase analysis (RCA) have been applied with great effect to heterogeneous organometallic mixtures as described in a recent well-designed experiment reported by Frenkel et al.[41] Unfortunately, these techniques are of limited utility in settings such as discussed here. Pyrolysis creates a mixture of random Co−N_x ($x = 0-4$) molecules where "standards" are unavailable. Indeed, the inherent limitation of EXAFS is its bulk-averaging nature, and these standard modes of analysis will forever be of limited utility for heterogeneous catalysis. Nonetheless, when taken into account in conjunction with the other analytical methodologies explored in this report, the EXAFS results correlate extremely well with ex situ XPS data. However, also akin to the previously described methods, the results remain somewhat ambiguous as to the true nature of the catalytically active site.

3.3.2.3. Δμ Analysis. The Δμ technique of XANES analysis effectively removes the bulk signal from standard EXAFS and allows for direct spectroscopic probing and observation of adsorbates on an electrocatalyst surface under in operando conditions. That is, the technique has the capability to remove unreactive species that contribute to the bulk signal and leaves behind a highly specific signal of the relevant adsorption processes in respect to both the adsorbate and adsorbing atom. This has been applied with great effect to elucidating the relationship of adsorption sites, electrocatalyst surface structure, and electrochemical potential toward H_{ads} and O_{ads} on Pt/C[27,28] and Pt−M/C (M = Co, Cr, Ru, etc.)[29−31] catalysts. Further, we have shown that this technique can be applied to heterogeneous catalysts (a mixed-phase Rh_xS_y/C chalcogenide)[33,34] to identify the active phase for ORR.

On the basis of this experience and coupled with the complete structural analysis (with the denoted inherent limitations) reported above, the Δμ method was applied to the in situ XANES data over the pertinent kinetic/diffusion-controlled region as ascertained from the RRDE studies. The results of this analysis ($\Delta\mu = \mu(V) - \mu(0.30\ V)$) is presented in Figure 16. While all three catalysts exhibit a large minimum peak, some interesting differences are apparent with regard to the maxima in the range ~12−40 eV past the edge. The 600 °C exhibits a "double peak" maximum. At 700 °C, this feature is still evident but somewhat muted. By the time a pyrolysis temperature of 800 °C has been reached, this double peak is replaced with a quickly decaying maximum apparent until 0.70 V.

Theoretical (calculated via FEFF8.0) Δμ signatures are presented in Figure 17. As outlined in the Experimental section, these spectra were calculated from analogous Co−N_4, Co−N_3, and Co−N_2 models derived from prior crystallographic data adjusted to the EXAFS fitting results according to the relationship: $\Delta\mu = \mu(CoN_x-O_{ads}) - \mu(CoN_x)$. In all cases, the double peak maximum is reproduced only by an "axial" (normal to the Co−N_x plane) adsorption of O(H) as expressed by the

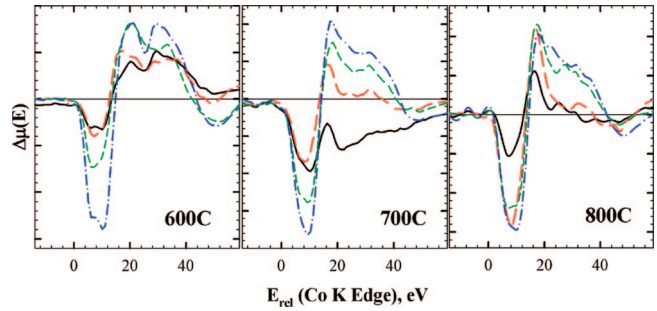

Figure 16. The experimental $\Delta\mu = \mu(V) - \mu(0.30\ V)$ curves for the pyrolyzed CoTMPP: 0.50 V (solid), 0.60 V (long dash), 0.70 V (short dash), and 0.80 V (dash−dot). Data was collected in situ (anodic scans) in 1 M TFMSA at a 20 mV s^{-1} scan rate.

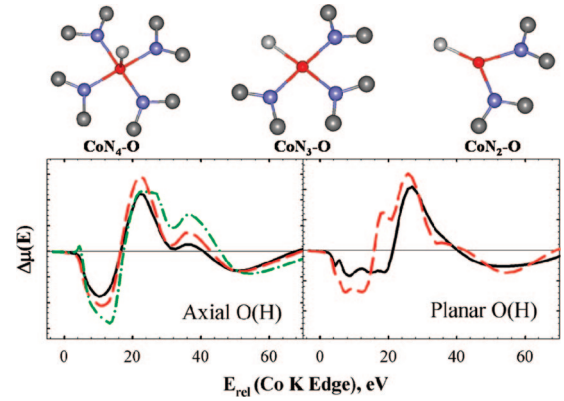

Figure 17. Top: representative models utilized for calculating the theoretical Δμ spectrum via FEFF8: (left) O_{axial} on Co−N_4, (center) O_{planar} on Co−N_3, (right) O_{planar} on Co−N_2. Bottom: FEFF8-generated theoretical $\Delta\mu = \mu(O_{ads}) - \mu(clean)$ spectra.

Co−N_4(O_{ads}) model in Figure 17. When the O_{ads} is situated in plane (i.e., "planar" O(H)) the resulting signal is a quickly decaying maximum following the initial minimum. While it is debatable that Co−N_3 would adsorb O in a planar or axial fashion, chemical intuition leads us to believe that axial adsorption of O is highly unlikely with a Co−N_2 site.

In contrast to the bulk N_{Co-N} coordination numbers derived from the XPS and Co K/L edge XAS results (Table 1), the Δμ analysis provides specific spectroscopic detail elucidating the nature and geometry of adsorbates on the Co−N_x active site, and the structure of the adsorption site greatly influences the spectrum. Removal of a nitrogen atom via pyrolysis from the plane of the Co−N_4 center results in O_{ads} in a planar geometry. Coupled with the substantial leap in the peroxide yield at 800 °C it is apparent that planar adsorption of molecular oxygen onto a Co−$N_{2/3}$ molecule results in a skewing of the ORR mechanism to the $2e^-$ peroxide pathway. A recent publication by Vayner et al.[55] utilized density functional theory calculations in conjunction with a linear Gibbs free energy relationship to probe the adsorption energies of various oxo-species on Co^{x+}−N fragments with respect to reversible electrochemical potential. This report was unavailable until recently, and it was a pleasant surprise to find that our experimental results are in agreement with the authors' rigorous theoretical assessment of a similar system. The spectroscopic fingerprinting of these electrocatalysts has provided the first report of the interrelationship between active site symmetry, O_{ads} geometry, and the ORR pathway.

4. Conclusion

The relevant structure/property relationships that affect the ORR pathway of unique self-supported pyrolyzed Co-based

porphyrin electrocatalysts (from silica-supported Co(II)TMPP precursors) was been elucidated through a combination of electrochemical and analytical techniques. All three pyrolyzed porphyrin electrocatalysts (600, 700, and 800 °C) show a highly porous graphitic structure via TEM analysis. Derivation of the electrochemical kinetics in 1 M perchloric acid provided parameters that indicate the material arising from the 700 °C pyrolysis provides for the highest performance. Most importantly, the RRDE experiments showed that the 800 °C material possessed a 10-fold increase in the peroxide yield. Ex situ XPS and Co L edge XAS analysis results were combined to show that the as-synthesized material contains significant domains of hcp Co and CoO_x deposits. However, these deposits do not survive the high-oxygen, low-pH environments of a PEMFC and do not contribute to the overall activity.

Co L/K edge XAS analysis agreed well with the electrochemical results in identifying a Co^{2+} reaction site. In situ EXAFS analysis showed that the planar (D_{4h} or S_4) character of the $Co-N_4$ portion of the CoTMPP precursor was reduced through increasing pyrolysis temperature but was retained in all of the studied electrocatalyst. These results offered decreasing extents of nitrogen coordination to the active Co^{2+} centers in respect to increasing pyrolysis temperature. Further, these modes of analysis suggest that the Co−N bond length decreases in respect to increasing pyrolysis temperature. All of these results were in agreement with previous reports in the literature.

Application of the $\Delta\mu$ technique (a specialized "difference XANES" process) to the in situ Co K edge XAS absorption spectra provided unprecedented insight into the nature of these materials. The $\Delta\mu$ technique allowed for the removal of bulk, unreactive processes from the in situ XAS data collected under potentiostatic conditions in 1 M $HClO_4$ and allowed for the direct spectroscopic observation of oxo species adsorption on the Cobased active sites. The unique signatures of these spectra showed that the increasing pyrolysis temperature resulted in an overall $Co-N_2$ active site by 800 °C. Correlation of the $\Delta\mu$ results with the structural bulk spectroscopic analyses, in addition to RRDE determinations of the peroxide yields, provides unambiguous proof that the level of N_{Co-N} coordination influences the oxygen reduction pathway.

The 600 and 700 °C materials retain a $Co-N_4$ stoichiometry and efficiently reduce oxygen to water to a full $4e^-$ pathway. In contrast, pyrolysis at 800 °C results in a bulk $Co-N_2$ structure and consequently results in a 10-fold mol % increase in peroxide production. It was the application of the $\Delta\mu$ technique to in situ Co K EXAFS data that supplied this level of detail. This is unique, for the $\Delta\mu$ process has thus far only been shown to function for materials that possess not only a clearly defined atomic structure (i.e., Pt and Rh_xS_y-based nanoparticles) but also a long developmental history in elucidating ORR mechanisms upon the relevant reactive surfaces. It is anticipated that the $\Delta\mu$ method can provide detailed information relating structure/property relationships to the (ORR) kinetic pathways of similar pyrolyzed, transition metal based organometallics.

Acknowledgment. Financial support was provided under the auspices of Multi-University Research Initiative grant from the Air Force Office of Scientific Research (contract FA9550-06-1-0264) administered by the University of New Mexico. The use of beamlines X-23A2 and U-7A at the National Synchrotron Light Source, Brookhaven National Laboratory, was supported by the U.S. Department of Energy, Office of Science, Office of Basic Energy Sciences, under Contract No. DE-AC02-98CH10886. Dr. Dino Villagran (MIT, Department of Chemistry) provided the high-purity Co(II)OEP.

Supporting Information Available: Figures encompassing additional electrochemical and XAS details. This material is available free of charge via the Internet at http://pubs.acs.org.

References and Notes

(1) Schmidt, T. J.; Paulus, U. A.; Gasteiger, H. A.; Behm, R. J. *J. Electroanal. Chem.* **2001**, *508*, 41.
(2) Shukla, A. K.; Raman, R. K. *Annu. Rev. Mater. Res.* **2003**, *33*, 155.
(3) Lipkowski, J.; Ross, P. N. *Electrocatalysis*; Wiley-VCH: New York, 1998; p 376.
(4) Marković, N. M.; Ross, P. N. *Surf. Sci. Rep.* **2002**, *45*, 117.
(5) Mukerjee, S. In *Catalysis and Electrocatalysis at Nanoparticle Surfaces*; Wieckowski, A., Savinova, E. R., Vayenas, C. G., Eds.; Marcel Dekker: New York, 2003; pp 501−531.
(6) Ross, P. N. In *Electrocatalysis*, Lipkowski, J., Ross, P. N., Eds. Wiley-VCH: New York, 1998; pp 43−74.
(7) Hwu, H. H.; Chen, J. G. *J. Phys. Chem. B* **2003**, *107*, 11467.
(8) Hwu, H. H.; Fruhberger, B.; Chen, J. G. *J. Catal.* **2004**, *221*, 170.
(9) Liu, N.; Kourtakis, K.; Figueroa, J. C.; Chen, J. G. *J. Catal.* **2003**, *215*, 254.
(10) Alonso-Vante, N. In *Catalysis and Electrocatalysis at Nanoparticle Surfaces*; Wieckowski, A., Savinova, E. R., Vayenas, C. G., Eds.; Marcel Dekker: New York, 2003; pp 931−958.
(11) Vante, A. N.; Tributsch, H. *Nature* **1986**, *323*, 431.
(12) Chang, C. J.; Zhi-Heng, L.; Shi, C.; Anson, F. C.; Nocera, D. C. *J. Am. Chem. Soc.* **2004**, *126*, 10013.
(13) Wang, B. *J. Power Sources* **2005**, *152*, 1.
(14) Dunford, H. B. *Heme Peroxidases*; Wiley-VCH: New York, 1999; p 528.
(15) Song, E.; Shi, C.; Anson, F. C. *Langmuir* **1998**, *14*, 4315.
(16) Cote, R.; Lalande, G.; Faubert, G.; Guay, D.; Dodelet, J. P.; Denes, G. *J. New Mater. Electrochem. Syst.* **1998**, *1*, 7.
(17) Gojkovic, S. L.; Gupta, S.; Savinell, R. F. *J. Electrochem. Soc.* **1998**, *145*, 3493.
(18) Gouérec, P.; Savy, M.; Riga, J. *Electrochim. Acta* **1998**, *43*, 743.
(19) Ladouceur, M.; Lalande, G.; Guay, D.; Dodelet, J. P.; Dignardbailey, L.; Trudeau, M. L.; Schulz, R. *J. Electrochem. Soc.* **1993**, *140*, 1974.
(20) van Veen, J. A. R.; van Baar, J. F.; Kroese, K. J. *J. Chem. Soc., Faraday Trans.* **1981**, *77*, 2827.
(21) Jiang, R.; Chu, D. *J. Electrochem. Soc.* **2000**, *147*, 4605.
(22) Yeager, E. J. *J. Mol. Catal.* **1986**, *38*, 5.
(23) Lalande, G.; Cote, R.; Tamizhmani, G.; Guay, D.; Dodelet, J. P.; Dignardbailey, L.; Weng, L. T.; Bertrand, P. *Electrochim. Acta* **1995**, *40*, 2635.
(24) Bouwkamp-Wijnoltz, A. L.; Visscher, W.; van Veen, J. A. R.; Boellaard, E.; van der Kraan, A. M.; Tang, S. C. *J. Phys. Chem. B* **2002**, *106*, 12993.
(25) Lefevre, M.; Dodelet, J. P.; Bertrand, P. *J. Phys. Chem. B* **2002**, *106*, 8705.
(26) Jaouen, F.; Marcotte, S.; Dodelet, J.-P.; Lindbergh, G. *J. Phys. Chem. B* **2003**, *107*, 1376.
(27) Teliska, M.; O'Grady, W. E.; Ramaker, D. E. *J. Phys. Chem. B* **2004**, *108*, 2333.
(28) Teliska, M.; O'Grady, W. E.; Ramaker, D. E. *J. Phys. Chem. B* **2005**, *109*, 8076.
(29) Teliska, M.; Murthi, V. S.; Mukerjee, S.; Ramaker, D. E. *J. Electrochem. Soc.* **2005**, *152*, A1259.
(30) Scott, F. J.; Mukerjee, S.; Ramaker, D. E. *J. Electrochem. Soc.* **2007**, *154*, A396.
(31) Roth, C.; Benker, N.; Buhrmester, T.; Mazurek, M.; Loster, M.; Fuess, H.; Koningsberger, D. C.; Ramaker, D. E. *J. Am. Chem. Soc.* **2005**, *127*, 14607.
(32) Scott, F. J.; Roth, C.; Ramaker, D. E. *J. Phys. Chem. C* **2007**, *111*, 11403.
(33) Ziegelbauer, J. M.; Gatewood, D.; Gullá, A. F.; Ramaker, D. E.; Mukerjee, S. *Electrochem. Solid-State Lett.* **2006**, *9*, A430.
(34) Ziegelbauer, J. M.; Gatewood, D.; Ramaker, D. E.; Mukerjee, S. *ECS Trans.* **2006**, *1*, 119.
(35) Paulus, U. A.; Schmidt, T. J.; Gasteiger, H. A.; Behm, R. J. *J. Electroanal. Chem.* **2001**, *495*, 134.
(36) Murthi, V. S.; Urian, R. C.; Mukerjee, S. *J. Phys. Chem. B* **2004**, *108*, 11011.
(37) Newville, M. *J. Synchrotron. Radiat.* **2001**, *8*, 322.
(38) Ressler, T. *J. Synchrotron. Radiat.* **1998**, *5*, 118.
(39) McBreen, J.; O'Grady, W. E.; Pandya, K. I.; Hoffman, R. W.; Sayers, D. E. *Langmuir* **1987**, *3*, 428.
(40) Koningsberger, D. C.; Mojet, B. I.; Van Dorssen, G. E.; Ramaker, D. E. *Top. Catal.* **2000**, *10*, 143.
(41) Frenkel, A. I.; LKleifeld, O.; Wasserman, S. R.; Sagi, I. *J. Chem. Phys.* **2002**, *116*, 9449.

(42) Madura, P.; Scheidt, W. R. *Inorg. Chem.* **1976**, *15*, 3152.
(43) Scheidt, W. R.; Turowska-Tyrk, I. *Inorg. Chem.* **1994**, *33*, 1314.
(44) Ankudinov, A. L.; Ravel, B.; Rehr, J. J.; Conradson, S. D. *Phys. Rev. B* **1998**, *58*, 7565.
(45) Artyushkova, K.; Levendoski, S.; Atanassov, P.; Fulghum, J. E. *Top. Catal.*, submitted.
(46) Gojkovic, S. J.; Gupta, S.; Savinell, R. F. *J. Electroanal. Chem.* **1999**, *462*, 63.
(47) Villers, D.; Jacques-Bedard, X.; Dodelet, J. P. *J. Electrochem. Soc.* **2004**, *151*, A1507.
(48) Sepa, D. B.; Vojnovic, M. V.; Damjanovic, A. *Electrochim. Acta* **1981**, *26*, 781.
(49) Olson, T. S.; Atanassov, P.; Chapman, K. Performance of Nano-Structured Non-Platinum Electrocatalysts for Oxygen Reduction in Fuel Cells. In *211th Meeting of the Electrochemical Society - Electrochemistry of Novel Electrode Materials for Energy Conversion and Storage*; The Electrochemical Society: Chicago, 2007.
(50) Chu, D.; Jiang, R. *Solid State Ionics* **2002**, *148*, 591.
(51) Chen, J. G. *Surf. Sci. Rep.* **1997**, *30*, 1.
(52) Cotton, F. A. *Chemical Applications of Group Theory*, 3rd ed.; Wiley: New York, 1990; p 480.
(53) Sagi, I.; Wirt, M. D.; Chen, E.; Frisbie, S. M.; Chance, M. R. *J. Am. Chem. Soc.* **1990**, *112*, 8639.
(54) Wirt, M. D.; Sagi, I.; Chance, M. R. *Biophys. J.* **1992**, *63*, 412.
(55) Vayner, E.; Anderson, A. B. *J. Phys. Chem. C* **2007**, *111*, 9330.

JP8001564